haematologica
Journal of the Ferrata Storti Foundation

Molecular landscape of *FLT3*-ITD mutations in a chemotherapy treated ECOG-ACRIN E1900 clinical trial

by Varsha Singh, Meredith Arterburn, Michael Bowman, Shreeya Gounder, Nisargbhai Shah, Hugo F. Fernandez, Martin S. Tallman, Janis Racevskis, Jacob M. Rowe, Hillard M. Lazarus, Mark R. Litzlow, Ari Melnick, Yanming Zhang, Ross L. Levine, Zhuoxin Sun, Selina M. Luger, Elisabeth M. Paietta and Robert L. Bowman

Received: August 20, 2026.
Accepted: November 13, 2026.

Citation: Varsha Singh, Meredith Arterburn, Michael Bowman, Shreeya Gounder, Nisargbhai Shah, Hugo F. Fernandez, Martin S. Tallman, Janis Racevskis, Jacob M. Rowe, Hillard M. Lazarus, Mark R. Litzlow, Ari Melnick, Yanming Zhang, Ross L. Levine, Zhuoxin Sun, Selina M. Luger, Elisabeth M. Paietta and Robert L. Bowman. Molecular landscape of FLT3-ITD mutations in a chemotherapy treated ECOG-ACRIN E1900 clinical trial. Haematologica. 2026 Nov 26. doi: 10.3324/haematol.2026.301839 [Epub ahead of print]

Publisher's Disclaimer.
E-publishing ahead of print is increasingly important for the rapid dissemination of science. Haematologica is, therefore, E-publishing PDF files of an early version of manuscripts that have completed a regular peer review and have been accepted for publication.
E-publishing of this PDF file has been approved by the authors.
After having E-published Ahead of Print, manuscripts will then undergo technical and English editing, typesetting, proof correction and be presented for the authors' final approval, the final version of the manuscript will then appear in a regular issue of the journal.
All legal disclaimers that apply to the journal also pertain to this production process.

Molecular landscape of *FLT3*-ITD mutations in a chemotherapy treated ECOG-ACRIN E1900 clinical trial

Short title: *FLT3*-ITD clonal architecture in AML

Varsha Singh[1], Meredith Arterburn[1], Michael Bowman[1], Shreeya Gounder[1], Nisargbhai Shah[1], Hugo F. Fernandez[2], Martin S. Tallman[3], Janis Racevskis[4], Jacob M. Rowe[5], Hillard M. Lazarus[6], Mark R. Litzow[7], Ari Melnick[8], Yanming Zhang[9], Ross L. Levine[3,10], Zhuoxin Sun[11], Selina M. Luger[12], Elisabeth M. Paietta[4], Robert L. Bowman[1#]

[1]Department of Cancer Biology, Perelman Cancer Center, University of Pennsylvania, Philadelphia, PA

[2]Department of Malignant Hematology and Cellular Therapy, H. Lee Moffitt Cancer Center, Pembroke Pines, FL.

[3]Leukemia Service, Dept. of Medicine, Memorial Sloan Kettering Cancer Center, New York, NY

[4]Montefiore Medical Center, Bronx, NY

[5]Shaare Zedek Medical Center, Jerusalem, Israel.

[6]Department of Medicine, University Hospitals Cleveland Medical Center, Case Western Reserve University, Cleveland, OH.

[7]Division of Hematology Mayo Clinic Rochester, MN 55902 USA.

[8]Institut de Recerca contra la Leucèmia Josep Carreras, Barcelona, Spain 08022.

[9]Department of Pathology, Memorial Sloan Kettering Cancer Center, New York, NY, USA.

[10]Molecular Cancer Medicine Service, Human Oncology and Pathogenesis Program, Leukemia service DOM, Memorial Sloan Kettering Cancer Center, New York, NY, USA.

[11]Dana-Farber Cancer Institute, Boston, MA, USA.

[12]Division of Hematology-Oncology, Abramson Cancer Center, University of Pennsylvania, Philadelphia, PA.

[#]Correspondence: Robert. L Bowman, Robert.bowman@pennmedicine.upenn.edu

ACKNOWLEDGMENTS: We are grateful to members of the Bowman lab, Dr. Martin Carroll and Dr. Alexander Perl for discussion. We acknowledge the High Throughput Sequencing Core at the Children's Hospital of Philadelphia for their assistance in sequencing. R.L.B was supported by the American Society of Hematology (ASH Scholar), V Foundation and the National Institute of Health (R37CA226433). This study was conducted by the ECOG-ACRIN Cancer Research Group (Peter J. O'Dwyer, MD and Mitchell D. Schnall, MD, PhD, Group Co-Chairs) and supported by the National Cancer Institute of the National Institutes of Health under award numbers: U10CA180827, U10CA180820, U10CA180794, UG1CA189859, UG1CA308623, UG1CA233290, UG1CA232760, UG1CA233332, UG1CA233234, and UG1CA233320. The content is solely the responsibility of the authors and does not necessarily represent the official views of the National Institutes of Health.

AUTHORSHIP CONTRIBUTIONS: V.S., S.L., J.M.R., E.P., R.L.L., and R.L.B. conceived and designed the study. H.F.F., M.S.T., H.M.L., M.R.L., performed clinical trial and project development. A.R., J.R., E.M.P., Z.S., Y.Z., were

responsible for specimen processing, clinical annotation, and clinical data management. V.S., M.A., M.B., S.G. and N.S. performed experiments and collected data. V.S., M.A., M.B., and R.L.B. analyzed, interpreted the data and made (1)figures. V.S., M.A., and R.L.B. drafted the manuscript. S.L., E.P., and R.L.B. provided critical resources, supervision, and scientific guidance. All authors reviewed, edited, and approved the final manuscript.

DISCLOSURE OF CONFLICTS OF INTEREST: H.M.L. has served as a promotional speaker or consultant for Seattle Genetics, Geron, Pfizer, Actinium Pharmaceuticals, Jazz Pharmaceuticals, Pluristem Therapeutics, Partner Therapeutics, CSL Behring and GlycoMimetics. H.M.L. as served on data safety and monitoring boards for Bristol-Myers Squibb and BioSight and holds stock options in Partner Therapeutics. R.L.L. is a former member of the Supervisory Board and current SAB member for Qiagen (compensation/equity), a board member of the Mark Foundation for Cancer Research, a former founder/board member at Ajax, and a former scientific advisor to Mission Bio, Kurome, Syndax, Scorpion, Zentalis, Jubilant, Auron, Prelude, and C4 Therapeutics; for each of these entities he received equity/compensation. He has received research support from the Cure Breast Cancer Foundation (with IP rights), Calico, Zentalis and Ajax, and has consulted/provided professional services for ECOG-ACRIN, Genome Canada, Goldman Sachs and Astra Zeneca.

DATA SHARING: Original data will be made available under reasonable request to the corresponding author in accordance with permission from ECOG-ACRIN guidelines.

ARTIFICIAL INTELLIGENCE: *Name of the aAI software platform, program, or tool:* PennChat

- *Version:* GPT 5.1
- *Manufacturer / Developer*: OpenAI:
- *Commercial or open-source status*: Open source
- *A brief description of how the aAI was used, the specific functions or prompts utilized, and the portions of the manuscript affected*: aAI tools were used to provide basic code building blocks for data visualization and suggested grammar changes in manuscript formatting.
- *Confirmation that the author(s) take full responsibility for the integrity of the content generated*: Confirm

MAIN TEXT

FLT3 internal tandem duplications (*FLT3*-ITD) occur in 20-25% of acute myeloid leukemia (AML) and are associated with increased relapse following standard induction chemotherapy(2). ITDs are not a single molecular entity: insertions vary in site, length, variant allelic fraction (VAF), and sub-clonal complexity. Conventional fragment analysis detects *FLT3*-ITD at 1–5% VAF sensitivity, capturing only the dominant clone(3). Deep NGS-based identification has revealed substantially greater sub-clonal complexity(4),(5), yet no study has comprehensively integrated insertion site, allelic burden, clonal complexity, and co-mutational context in a uniformly treated, *FLT3*-inhibitor-free cohort. The ECOG-ACRIN E1900 trial (NCT00049517, 2002–2008) randomised adults ≤60 years with newly diagnosed AML to standard (45 mg/m2) or high-dose (90 mg/m2) daunorubicin plus cytarabine(6, 7), and provides a chemotherapy-only cohort in which these *FLT3*-ITD intrinsic molecular features can be evaluated. This cohort has undergone extensive clinical follow-up and molecular profiling offering high yield correlative information, despite changes in clinical care since completion of the trial. Here, we used deep NGS to characterize *FLT3*-ITD features in 127 *FLT3*-ITD-positive patients from E1900. We evaluated insertion site and length, allelic burden, subclonal contribution, and clonal diversity using Shannon entropy, and examined their associations with overall survival (OS) and event-free survival (EFS). The study was conducted in accordance with the Declaration of Helsinki and approved by IRB protocol #858882.

We identified 147 AML patients from ECOG-ACRIN E1900 with *FLT3*-ITD-positive disease indicated by clinical fragment analysis, 127 of which had DNA available for NGS. (*Supplementary Fig. 1A*). DNA from bone marrow or peripheral blood (50ng) at diagnosis was used as input for amplicon PCR for *FLT3* exons 14-15 as previously described(4). Libraries were sequenced on an Illumina NextSeq 2000 (P1 XLEAP-SBS, 600 cycles, 100M reads) with dual unique indexes and analyzed using the getITD workflow (v1.5.1, default parameters)(4). The previously established limit of detection for this assay is 0.0067% VAF(4). Two samples displayed a *FLT3*-ITD below this threshold and were subsequently excluded from analysis (*Supplementary Fig. 1B).* We characterized the mutational landscape of *FLT3*-ITD in this cohort by quantifying insertion site, length, and allelic burden at the event and patient levels. Sequencing depth was uniformly high across the cohort, with the majority of samples (>93%) achieving a median per-amplicon coverage exceeding 250,000 reads (*Supplementary Fig. 1C*). Deep sequencing identified 946 individual ITD events across 125 patients, comprising 390 unique ITD sequences (*Fig. 1A*), substantially exceeding conventional fragment analysis. The number of distinct ITD clones per patient ranged from 1 to 27 (median, 6; *Fig. 1B*), and ITD insertion length ranged from 6 to 266 nucleotides (median, 54 nt), with the 75-nt insertion being the most frequently observed (124 events; *Fig. 1C*).

We mapped detected ITD events to *FLT3* protein domains ITDs: including the JMD (aa 573–609) or TKD1 (aa 610–645; UniProt P36888). The JMD was the predominant insertion site (697/946 events, 73.7%), with the zipper motif (aa 580–600) accounting for 412 events (43.6%) and representing the most frequently disrupted subregion. Intronic and TKD1 insertions accounted for 140 (14.8%) and 109 (11.5%) events, respectively (*Supplementary Fig. 2A*). At the patient level, 62 (49.6%) had ITDs exclusively within the JMD, 57 (45.6%) had mixed-domain insertions spanning JMD and TKD1 with or without intronic involvement, and 3 (2.4%) each had TKD1-only or intron-only insertions.

Mixed-domain patients had significantly longer ITDs than JMD-only patients (p<0.001; *Supplementary Fig. 2B*). Among the 20 most frequently shared ITD sequences, 17 were in the JMD; the most prevalent was a 75-nt JMD zipper insertion shared by 78 patients, median per-patient VAF of 0.11% (*Fig. 1D*). Max VAF was comparable between JMD-only and mixed-domain patients (*Supplementary Fig. 2C*), whereas mixed-domain patients had greater subclonal allelic burden than JMD-only patients (median, 4.5% vs. 1.1%; p<0.003; *Supplementary Fig. 2D*). Across all 946 ITD events, VAF ranged from 0.006-100% (median, 0.074%), with most clones present at <1% VAF (*Fig. 1E*). Together, these findings demonstrate extensive structural and subclonal heterogeneity of *FLT3*-ITD at diagnosis.

Given that nearly all patients (97.6%) harbored multiple ITD mutations, we sought to quantify intra-patient clonal diversity using Shannon entropy (H; range=0-2.14; median=0.59). Patients were classified as monoclonal (H<0.3; n=49, 39.2%), oligoclonal (0.3≤H<1.2; n=62, 49.6%), or polyclonal (H≥1.2; n=14, 11.2%) (*Fig. 2A*). Clonality class correlated with ITD clone count (Spearman ρ=0.64, <0.001; median clones, 4, 7, and 14 for monoclonal, oligoclonal, and polyclonal groups, respectively) and with subclonal VAF contribution (ρ=0.72, p<0.001), supporting entropy as a measure of difference in clonal architecture (*Fig. 2B–D; Supplementary Fig. 3A*). Shannon entropy was inversely correlated with max VAF (ρ=−0.39, p<0.001), indicating that greater clonal diversity was associated with less allelic dominance by a single clone (*Supplementary Fig. 3B*). While ITD insertion length did not differ across clonality classes (p<0.087; *Supplementary Fig. 3C*), domain category was associated with clonal complexity, with mixed-domain patients showing the highest complexity (p<0.013; *Supplementary Fig. 3D*). Analysis of a previously characterized(8) limited set of co-mutations (n=11) showed no consistent association with *FLT3* molecular features; however adverse karyotype was associated with lower Shannon entropy and fewer ITD clones per patient (median H, 0.10 vs. 0.70, p<0.005; median clones, 3 vs. 7, p<0.001) (*Fig. 2E, Supplementary Fig. 3E*). Together, these findings establish Shannon entropy as a complementary measure of *FLT3*-ITD clonal architecture that captures differences in subclonal representation beyond clone count or dominant-clone VAF.

We next examined whether structural and allelic features of *FLT3*-ITD were associated with clinical outcome. While a univariate model demonstrated that patients with mixed-domain ITDs had inferior OS compared with those with JMD-only ITDs (median, 10.2 vs. 13.8 months; HR 1.60, 95% CI 1.08–2.38; p<0.02); this association was not found in a multivariate model considering treatment regimen (OS HR 1.5, 95% CI 1.00-2.25, p<0.052). Max VAF above cohort median (18.6%), had inferior OS compared with lower VAF (HR 1.60, 95% CI 1.08–2.37; p<0.017), whereas EFS did not differ (p<0.29). The cohort-median cutpoint was pre-specified to avoid optimised threshold selection, as continuous VAF showed only a borderline association with OS (HR 1.008 per 1% increase, 95% CI 0.999–1.017; p<0.074). We observed high concordance between max VAF and allelic ratio (AR; *Supplementary Fig. 3F*). While we found that the previous ELN AR threshold ≥0.5 was not associated with OS (p<0.11), AR dichotomized at the cohort median (AR≥0.228) identified patients with inferior OS (p<0.017) similar to VAF.

Ultimately, these univariate associations were abolished upon adjustment for clinical covariates. Mixed-domain ITDs were more frequent in the standard-dose arm (55.6% vs. 32.1%), and after adjustment for treatment arm these associations were no longer significant (OS HR 1.50, 95% CI 0.997–2.25, p=0.052; EFS HR 1.47, 95% CI 0.99–2.18,

p=0.057). In a multivariable Cox model including ITD domain, allelic burden, AR, co-mutation burden, Shannon entropy, age, ECOG performance status and treatment arm (n=118), no *FLT3*-ITD molecular feature associated with outcome. ECOG performance status was the only independent predictor of EFS (HR, 1.57,95% CI 1.12–2.19; p=0.009; *Fig. 3*). Subgroup analyses further confirmed that max VAF did not independently predict OS in *NPM1*-mutated (n=45; Cox HR 1.004, 95% CI 0.99–1.02, p<0.64) or adverse karyotype patients (n=25; Cox HR 1.017, 95% CI 1.00–1.04, p<0.10). Collectively, these data indicate that the prognostic significance of *FLT3*-ITD structural and allelic features is confounded by their skewed distribution across genetic, cytogenetic, and treatment contexts.

Taken together, deep sequencing revealed extensive structural and clonal heterogeneity of *FLT3*-ITD in AML, including substantial subclonal allelic diversity captured by Shannon entropy. This study demonstrates that *FLT3*-ITD structural and clonal complexity at diagnosis substantially exceeds what is detectable by conventional fragment analysis. The near-universal detection of multiple ITD clones (97.6%) at a median of 6 clones per patient suggests that multiclonal *FLT3*-ITD architecture is common event in *FLT3*-mutant AML. The 75-nt JMD zipper insertion shared across the majority of patients further highlights recurrent structural patterns within *FLT3*-ITD. Shannon entropy provides a quantitative framework for capturing differences in subclonal architecture beyond clone count alone. While the association between adverse karyotype and lower clonal entropy suggests distinct patterns of disease architecture, the coverage of co-mutational partners is insufficient to definitively determine their relationship with *FLT3*-ITD molecular findings.

Consistent with prior observations(9),(1), mixed-domain insertions and higher allelic burden were associated with inferior OS in univariate analyses, however these associations were not independently significant after multivariable adjustment. The imbalance in JMD distribution between treatment arms represents an additional confounding factor that may partly explain the univariate domain association. Further treatment advances since the conclusion of ECOG-ACRIN E1900 should caution against extrapolating the prognostic relevance of *FLT3*-ITD molecular features from this study to more contemporary treatment regimens. Despite these complications, this pre-*FLT3* inhibitor cohort provides an important molecular reference for contemporary *FLT3*-targeted trials, including PrE0905, and supports integrating *FLT3*-ITD structure, allelic burden, and clonal architecture with longitudinal monitoring(10, 11). Recent studies have demonstrated NGS-detected *FLT3*-ITD microclones can contribute to relapse through expansion of diagnostic subclones(12), while residual *FLT3*-ITD burden and multiclonal persistence during MRD assessment are associated with relapse and survival(10, 11). Thus, serial assessment of *FLT3*-ITD burden and clonal composition may provide greater prognostic value than diagnostic measurements alone.

REFERENCES:

1. Kayser S, Schlenk RF, Londono MC, et al. Insertion of FLT3 internal tandem duplication in the tyrosine kinase domain-1 is associated with resistance to chemotherapy and inferior outcome. Blood. 2009;114(12):2386-2392.

2. Döhner H, Wei AH, Appelbaum FR, et al. Diagnosis and management of AML in adults: 2022 recommendations from an international expert panel on behalf of the ELN. Blood. 2022;140(12):1345-1377.

3. Polak TB, van Rosmalen J, Dirven S, et al. Association of internal tandem duplication length with overall survival in acute myeloid leukemia: a systematic review and meta-analysis. Haematologica. 2022;107(10):2506-2510.

4. Blatte TJ, Schmalbrock LK, Skambraks S, et al. getITD for FLT3-ITD-based MRD monitoring in AML. Leukemia. 2019;33(10):2535-2539.

5. Schranz K, Hubmann M, Harin E, et al. Clonal heterogeneity of FLT3-ITD detected by high-throughput amplicon sequencing correlates with adverse prognosis in acute myeloid leukemia. Oncotarget. 2018;9(53):30128-30145.

6. Fernandez HF, Sun ZX, Yao XP, et al. Anthracycline dose intensification in acute myeloid leukemia. New Engl J Med. 2009;361(13):1249-1259.

7. Luskin MR, Lee JW, Fernandez HF, et al. Benefit of high-dose daunorubicin in AML induction extends across cytogenetic and molecular groups. Blood. 2016;127(12):1551-1558.

8. Patel JP, Gonen M, Figueroa ME, et al. Prognostic relevance of integrated genetic profiling in acute myeloid leukemia. N Engl J Med. 2012;366(12):1079-1089.

9. Rücker FG, Du L, Luck TJ, et al. Molecular landscape and prognostic impact of FLT3-ITD insertion site in acute myeloid leukemia: RATIFY study results. Leukemia. 2022;36(1):90-99.

10. Dillon LW, Gui G, Ravindra N, et al. Measurable residual FLT3 internal tandem duplication before allogeneic transplant for acute myeloid leukemia. JAMA Oncol. 2024;10(8):1104-1110.

11. Levis MJ, Hamadani M, Logan BR, et al. Measurable residual disease and posttransplantation gilteritinib maintenance for patients with FLT3-ITD-mutated AML. Blood. 2025;145(19):2138-2148.

12. Duployez N, Joudinaud R, Boudry A, et al. Prognostic impact of FLT3-ITD microclones in young adults with acute myeloid leukemia treated with intensive chemotherapy. Blood. 2026;148(5):598-609.

Figure 1. *FLT3*-ITD molecular landscape. (A) Bar chart showing *FLT3*-ITD recurrence pattern — the number of ITD sequences shared by exactly one patient (individual, blue) vs. two or more patients (shared, red). The majority of ITD sequences are individual; a subset of dominant sequences are shared across multiple patients, reflecting convergent ITD acquisition. **(B)** Histogram of the number of distinct ITD clones per patient (median 6, range 1–27), demonstrating marked inter-patient heterogeneity in clonal complexity. **(C)** Histogram of ITD insertion length distribution across all 946 ITD events (range 6–266nt, median 54nt), coloured by domain (Intron = yellow, JMD = blue, TKD = red). The distribution is right skewed with a prominent peak at 75 nt. **(D)** Box-and-jitter plot of per-patient VAF distribution (log_{10} scale) for each of the top 20 most frequently shared *FLT3*-ITD sequences, ranked by number of patients sharing the ITD. Each dot represents one patient. Labels indicate ITD length and patient count. Coloured by domain. **(E)** Histogram of all 946 individual ITD VAFs on a log_{10} scale, coloured by domain. Median per-event VAF = 0.074%; 75th percentile = 0.88%. Dashed vertical lines indicate clinical VAF thresholds of 0.06%, 1%, and 2%.

Figure 2. *FLT3*-ITD clonal complexity quantified using Shannon Entropy. (A) Histogram of Shannon entropy (H) per patient, coloured by clonality class: Monoclonal ($H < 0.3$, n = 49, 39.2%, blue), Oligoclonal ($0.3 \leq H < 1.2$, n = 62, 49.6%, yellow), Polyclonal ($H \geq 1.2$, n = 14, 11.2%, red). Dashed vertical lines indicate classification thresholds at H = 0.3 and H = 1.2. **(B)** Scatter plot of ITD clone count per patient (x-axis) vs. Shannon entropy (y-axis), coloured by clonality class. Each point represents one patient. Spearman $\rho = 0.64$, $p < 0.001$. Grey line with shading shows linear regression with 95% confidence interval. **(C)** Box-and-jitter plot of ITD clone count by clonality class. Median clone count increased progressively: 4 clones (Monoclonal), 7 clones (Oligoclonal), and 14 clones (Polyclonal), confirming that Shannon entropy identifies differences in ITD clonal architecture. **(D)** Box-and-jitter plot of sub-clonal ITD VAF contribution by clonality class. Sub-clonal burden was significantly higher in Polyclonal (median 12.4%) and Oligoclonal patients (median 9.8%) compared to Monoclonal patients (median 0.15%; Kruskal-Wallis $p < 0.001$). Spearman correlation between sub-clonal VAF contribution and Shannon entropy: $\rho = 0.72$, $p < 0.001$. **(E)** Box-and-jitter plots of Shannon entropy stratified by wildtype (WT) vs. mutated (Mut) status for each of nine individual co-mutations and adverse karyotype: *DNMT3A, NPM1, WT1, TET2, IDH2, Karyotype, MLL fusion, IDH1, ASXL1*. Mann-Whitney p-values shown above each panel..

Figure 3. Multivariable Cox regression of *FLT3*-ITD features and clinical variables on survival. Hazard ratios (HR, points) with 95% confidence intervals (bars) are shown on a log scale for overall survival (OS, left) and event-free survival (EFS, right). The analysis included patients with JMD-only (n=62) or mixed-domain (n=56) ITDs (n=118); 1 patient with missing ECOG performance status was excluded, leaving 118 patients in the models, TKD-only and intron-only cases (n=3 each) were excluded because of small numbers. Covariates were ITD domain (mixed vs JMD-only), maximum VAF (high vs low, cohort median 18.6%), co-mutation burden (per additional mutation), Shannon entropy (per unit), age (per year), ECOG performance status (per unit) and treatment arm regimen B (high-dose daunorubicin; n=51) vs A (standard-dose daunorubicin; n=67). Maximum allelic ratio (high vs low, cohort median 0.228) was analyzed in a parallel model in place of maximum VAF; the two metrics define

identical groups and give identical estimates. No *FLT3*-ITD feature was independently associated with OS or EFS. ECOG performance status was the only independent predictor of EFS (HR 1.57, 95% CI 1.12–2.19; p=0.009). Red indicates $p<0.05$; grey indicates $p\geq0.05$. Dashed line, HR=1; labels show HR (95% CI) and P value.

Figure 1

125 FLT3–ITD+ AML patients | 946 individual ITD events | 390 unique sequences

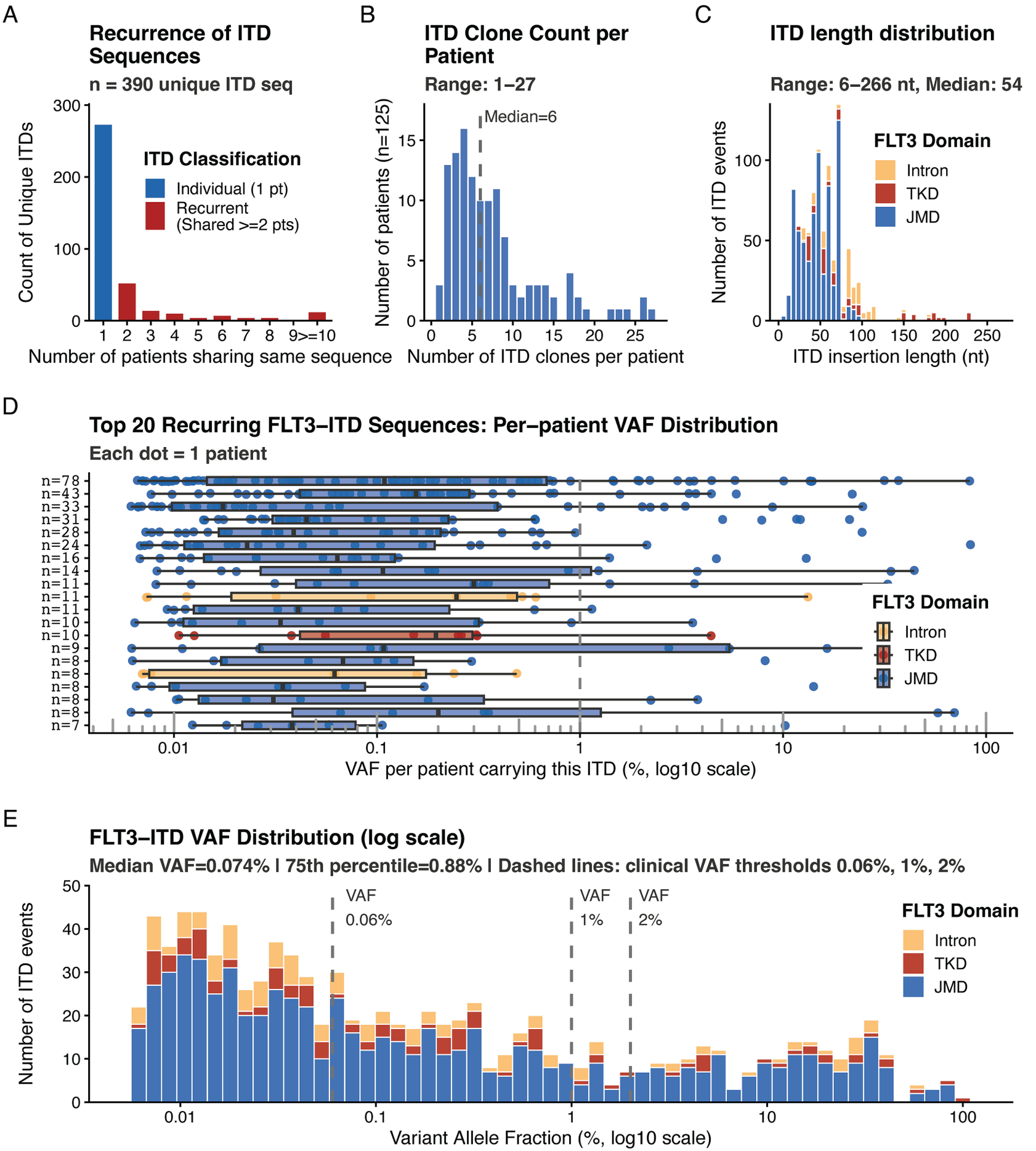
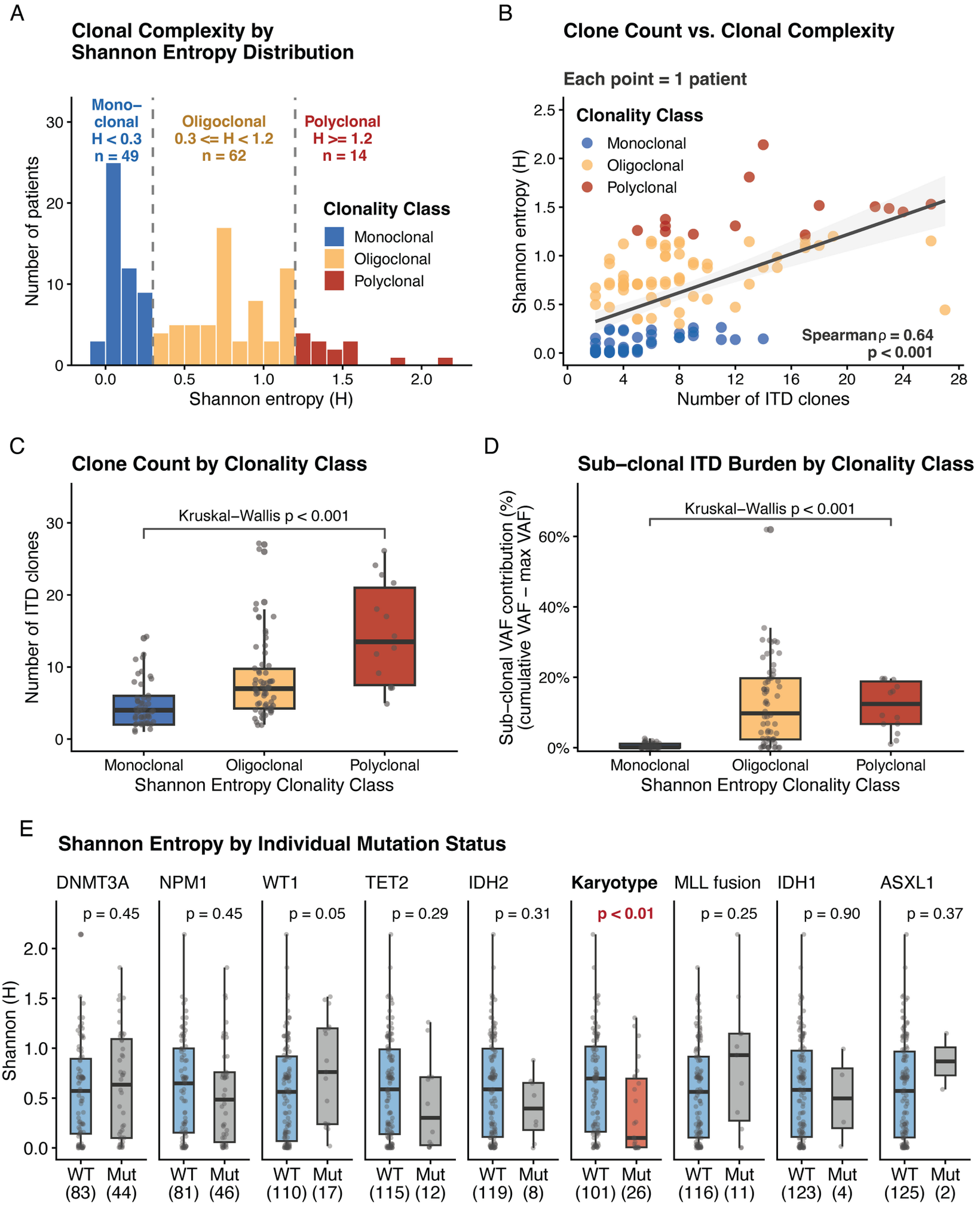
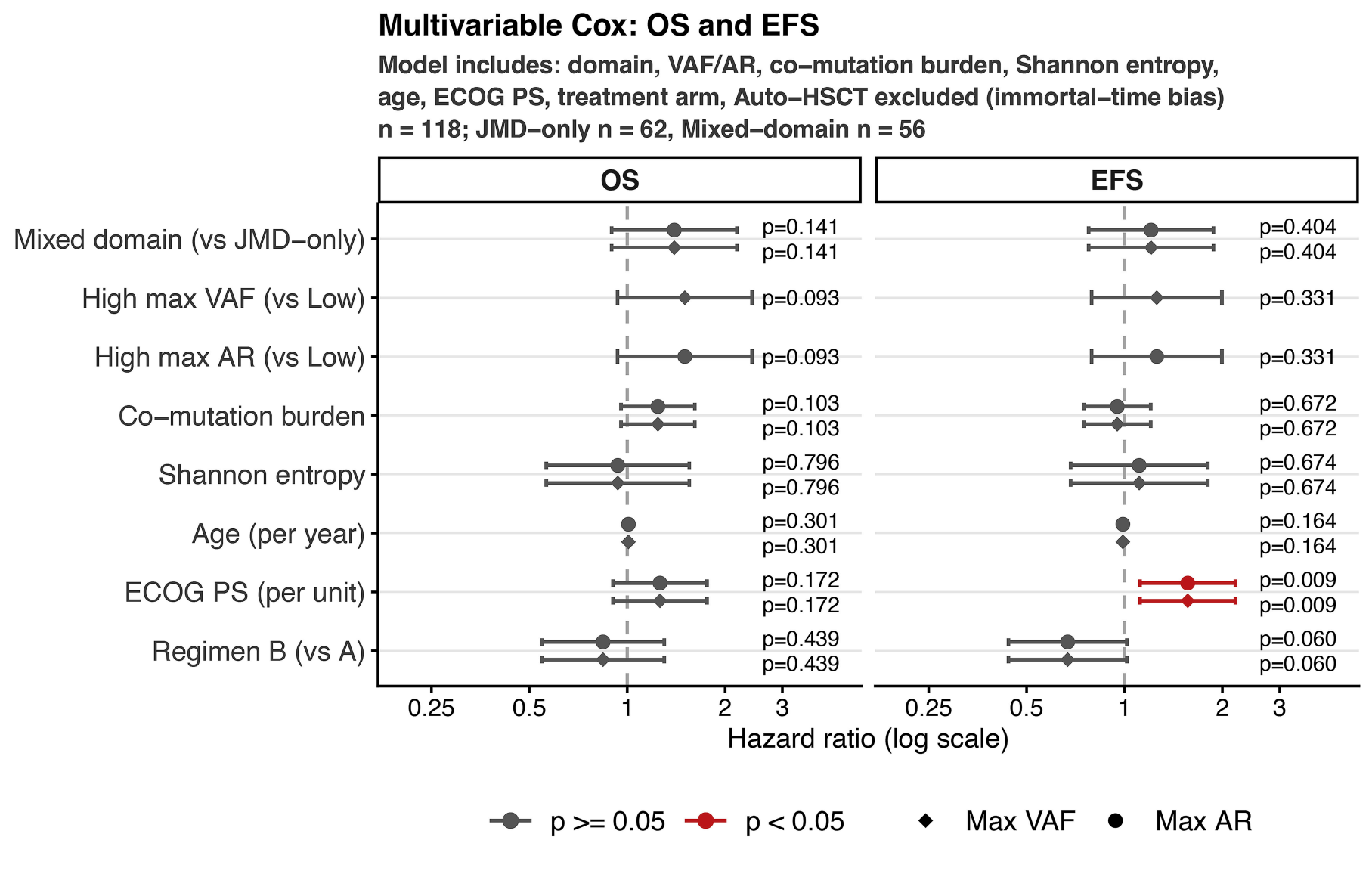
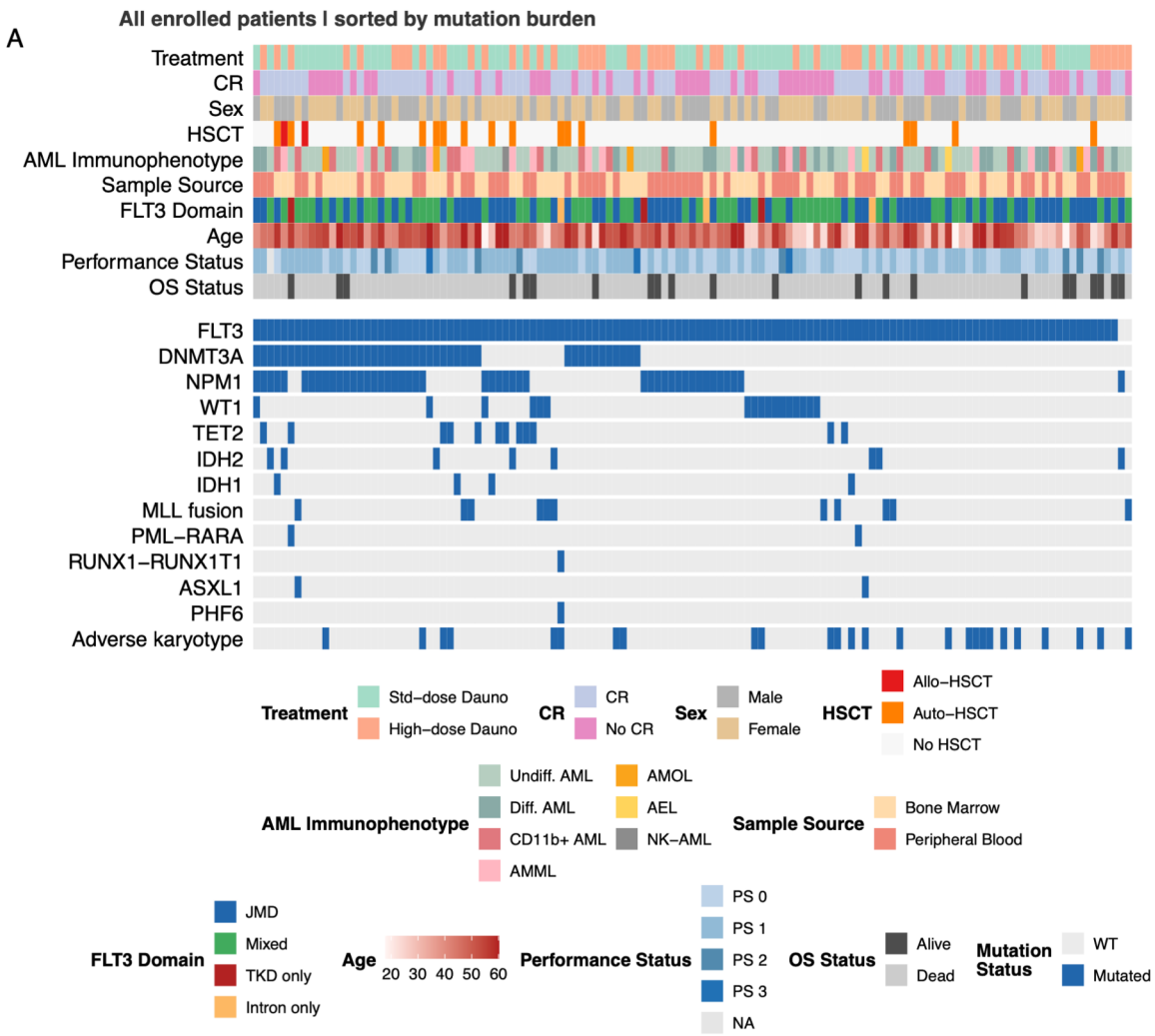


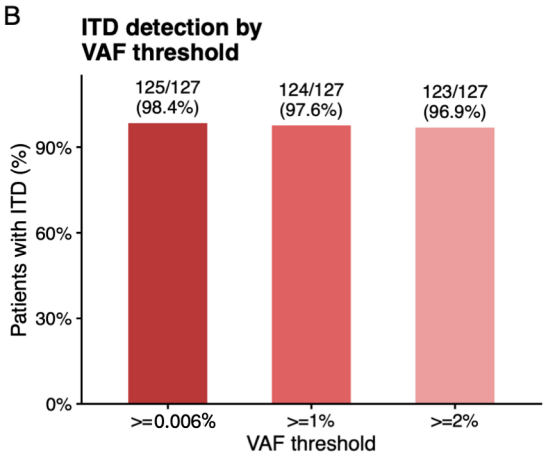
Figure 2

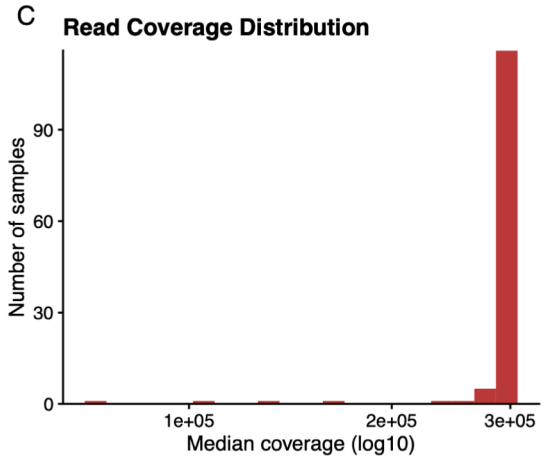

A
Clonal Complexity by Shannon Entropy Distribution
Mono–clonal H < 0.3 n = 49
Oligoclonal 0.3 <= H < 1.2 n = 62
Polyclonal H >= 1.2 n = 14
Clonality Class
Monoclonal
Oligoclonal
Polyclonal
Number of patients
Shannon entropy (H)
B
Clone Count vs. Clonal Complexity
Each point = 1 patient
Clonality Class
Monoclonal
Oligoclonal
Polyclonal
Shannon entropy (H)
Spearman ρ = 0.64
p < 0.001
Number of ITD clones
C
Clone Count by Clonality Class
Kruskal–Wallis p < 0.001
Number of ITD clones
Monoclonal
Oligoclonal
Polyclonal
Shannon Entropy Clonality Class
D
Sub–clonal ITD Burden by Clonality Class
Kruskal–Wallis p < 0.001
Sub–clonal VAF contribution (%) (cumulative VAF – max VAF)
Monoclonal
Oligoclonal
Polyclonal
Shannon Entropy Clonality Class
E
Shannon Entropy by Individual Mutation Status
DNMT3A p = 0.45 WT (83) Mut (44)
NPM1 p = 0.45 WT (81) Mut (46)
WT1 p = 0.05 WT (110) Mut (17)
TET2 p = 0.29 WT (115) Mut (12)
IDH2 p = 0.31 WT (119) Mut (8)
Karyotype p < 0.01 WT (101) Mut (26)
MLL fusion p = 0.25 WT (116) Mut (11)
IDH1 p = 0.90 WT (123) Mut (4)
ASXL1 p = 0.37 WT (125) Mut (2)
Shannon (H)


Multivariable Cox: OS and EFS
Model includes: domain, VAF/AR, co−mutation burden, Shannon entropy, age, ECOG PS, treatment arm, Auto−HSCT excluded (immortal−time bias)
n = 118; JMD−only n = 62, Mixed−domain n = 56
OS
EFS
Mixed domain (vs JMD−only)
High max VAF (vs Low)
High max AR (vs Low)
Co−mutation burden
Shannon entropy
Age (per year)
ECOG PS (per unit)
Regimen B (vs A)
p=0.141
p=0.141
p=0.404
p=0.404
p=0.093
p=0.331
p=0.093
p=0.331
p=0.103
p=0.103
p=0.672
p=0.672
p=0.796
p=0.796
p=0.674
p=0.674
p=0.301
p=0.301
p=0.164
p=0.164
p=0.172
p=0.172
p=0.009
p=0.009
p=0.439
p=0.439
p=0.060
p=0.060
0.25
0.5
1
2
3
Hazard ratio (log scale)
p >= 0.05
p < 0.05
Max VAF
Max AR

Supplementary Figure 1: Patient Profile and ITD Sequencing

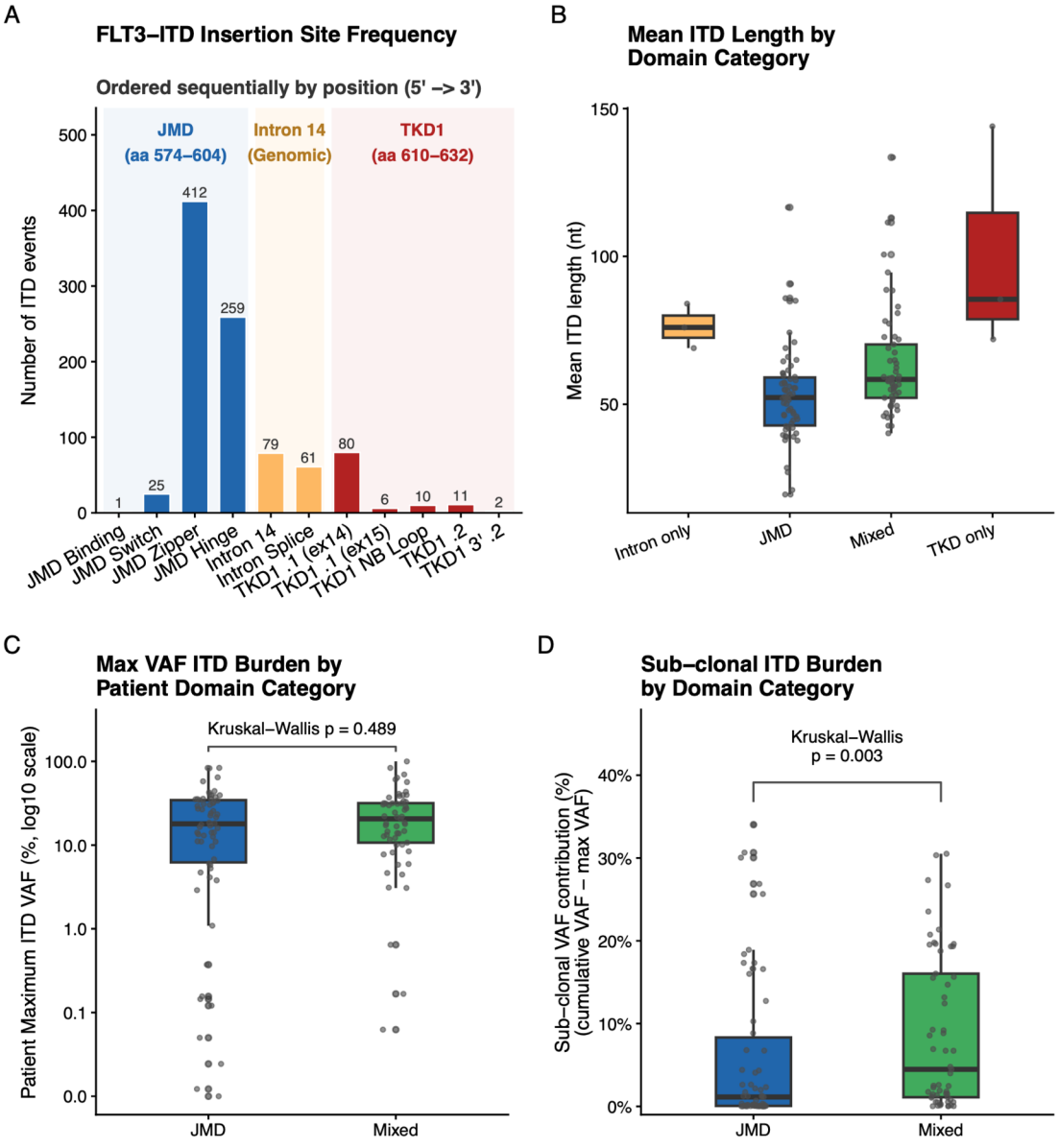






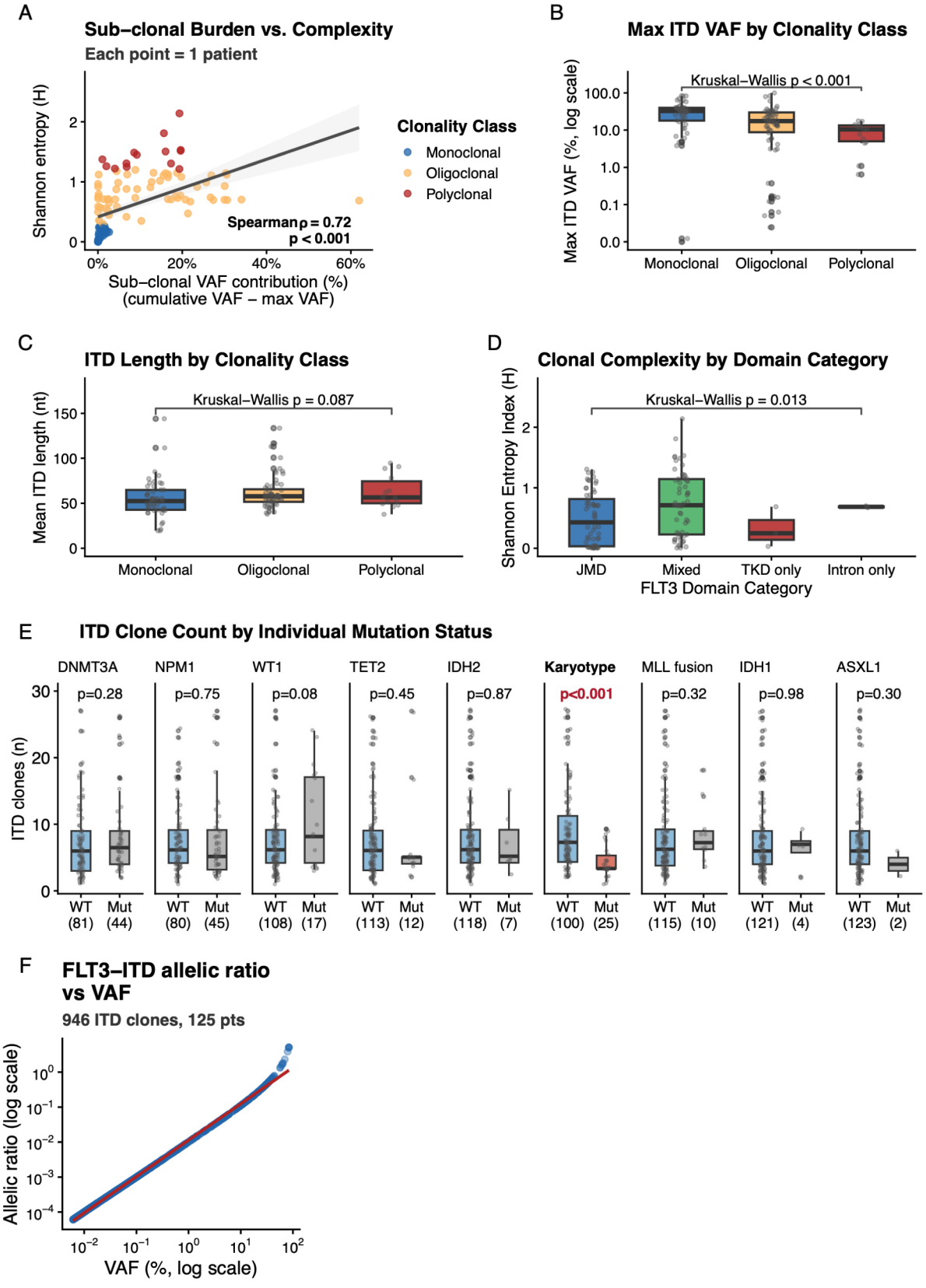
Supplementary Figure 1. Patient profile, sequencing coverage, and FLT3-ITD detection. (A) OncoPrint depicting the co-mutational and clinical landscape of all 127 enrolled patients, sorted by descending mutation burden. Each column represents one patient. Upper clinical annotation strips show: Treatment arm (standard-dose daunorubicin, n=72; high-dose daunorubicin, n=53; p<0.008 for CR rate); CR status (CR, n=69, 55.2%; No CR, n=56, 44.8%); Sex (Male, n=59, 47.2%; Female, n=66, 52.8%; p<0.362); HSCT status (Allo-HSCT, n=2; Auto-HSCT, n=18; No HSCT, n=107); AML immunophenotype (Undiff. AML = most frequent, n=58, 45.7%; Diff. AML; CD11b+ AML; AMOL; AEL; NK-AML; AMML); Sample source (Bone Marrow, n=62, 48.8%; Peripheral Blood, n=65, 51.2%); FLT3 domain category (JMD only, n=62, 49.6%; Mixed domain, n=57, 45.6%; TKD only, n=3, 2.4%; Intron only, n=3, 2.4%; p<0.05 between treatment arms)*, Domain distribution was imbalanced between treatment arms (Mixed domain 55.6% in Regimen A vs. 32.1% in Regimen B; p<0.05), representing a potential confounding factor for the observed univariate association between insertion domain and survival.*; Age (continuous gradient, range 18–60 years, mean 44.5 years); Performance status (PS 0, n=49, 39.5%; PS 1, n=64, 51.6%; PS 2, n=8, 6.5%; PS 3, n=3, 2.4%; p<0.076); OS status (black = Alive; grey = Dead). Lower panel shows mutation status (blue = Mutated; grey = Wild-type), DNMT3A (n=44, 34.6%), NPM1 (n=46, 36.2%), WT1 (n=17, 13.4%), TET2 (n=12, 9.4%), IDH2 (n=8, 6.3%), IDH1 (n=4, 3.1%), MLL fusion (n=11, 8.7%), PML-RARA (n=2, 1.6%), RUNX1-RUNX1T1 (n=2, 1.6%), ASXL1 (n=2, 1.6%), PHF6 (n=2, 1.6%), and adverse karyotype (n=25, 19.7%). **(B)** Bar chart of *FLT3*-ITD detection rates at three VAF thresholds: ≥0.06% (125/127, 98.4%), ≥1% (124/127, 97.6%), and ≥2% (123/127, 96.9%), confirming robust detection sensitivity across all clinically relevant thresholds. **(C)** Coverage distribution histogram showing median per-amplicon sequencing depth across all samples ($\log_{10}$ scale). Majority of samples achieved median coverage exceeding 250,000× reads.

Supplementary Figure 2: FLT3–ITD structural metrics



Supplementary Figure 2. *FLT3*-ITD structural metrics. (A) *FLT3*-ITD insertion site map across *FLT3* exons 14–15 (amino acid positions 573–645). Each bar represents a unique sub-region insertion site, ordered from exon 14 to 15. Annotated sub-regions include the JMD zipper motif (aa 573–600), hinge, switch and binding motifs, and TKD1 (aa 610–645). The JMD zipper motif at aa 580–600 accounts for the highest density of insertion events. **(B)** Box-and-jitter plot of mean ITD insertion length by patient- level domain category: Intron only, JMD, Mixed, and TKD only. TKD only patients showed the longest median insertion length, while JMD only patients showed the shortest. **(C)** Box-and-jitter plot of maximum ITD VAF per patient stratified by domain category (JMD only vs. Mixed domain). Maximum allelic burden was comparable between groups (Kruskal-Wallis $p < 0.489$), confirming that domain category and allelic burden represent independent axes of *FLT3*-ITD heterogeneity. **(D)** Box-and-jitter plot of sub-clonal *FLT3*-ITD allelic burden by domain category (JMD only vs. Mixed domain). Sub-clonal VAF contribution is defined as cumulative ITD VAF minus maximum clone VAF per patient. JMD only patients had a significantly lower sub-clonal burden (median 1.1%) compared to Mixed domain patients (median 4.5%; Kruskal-Wallis $p < 0.003$), indicating that structural and clonal complexity co-occur in the most genomically complex cases.

Supplementary Figure 3: Extended FLT3–ITD Clonal Complexity Analysis



Supplementary Figure 3. Extended *FLT3*-ITD clonal complexity and allelic ratio analysis. Panels A–E: Extended clonal complexity analyses. Panels F–H: Allelic ratio and survival analyses. For panels G–H: Kaplan-Meier curves with dashed lines indicating median survival, shaded regions representing 95% confidence intervals, and number at risk shown below each plot. **(A)** Scatter plot of Sub-clonal VAF per patient (x-axis) vs. Shannon entropy (y-axis), coloured by clonality class. Each point represents one patient. Spearman $\rho = 0.72$, $p < 0.001$. Grey line with shading shows linear regression with 95% confidence interval. **(B)** Box-and-jitter plot of maximum ITD VAF by clonality class (Monoclonal, Oligoclonal, Polyclonal). Max ITD VAF was significantly lower in sub-clonal and polyclonal classes compared to monoclonal (Kruskal- Wallis $p < 0.001$). **(C)** Box-and-jitter plot of mean ITD insertion length by clonality class. ITD insertion length did not significantly differ across clonality classes ($p< 0.087$), suggesting that clonal diversity is driven by sub-clonal variation in VAF rather than structural differences in the ITD itself. **(D)** Box-and-jitter plot of Shannon entropy by domain category (JMD, Mixed, TKD only, Intron only). Shannon entropy was significantly higher in Mixed domain patients compared to JMD only patients (Kruskal-Wallis $p< 0.013$), consistent with the greater clonal complexity of multi-domain insertions. **(E)** Box-and-jitter plots of ITD clone count stratified by wildtype (WT, blue) vs. mutated (Mut, grey) status for each of nine individual co-mutations and adverse karyotype: *DNMT3A* (WT n = 83, Mut n = 44, $p< 0.20$), *NPM1* (WT n = 81, Mut n = 46, $p< 0.69$), *WT1* (WT n = 110, Mut n = 17, $p< 0.06$), *TET2* (WT n = 115, Mut n = 12, $p< 0.52$), *IDH2* (WT n = 119, Mut n = 8, $p< 0.48$), Karyotype (WT n = 101, Mut n = 26, $p < 0.001$), *MLL fusion* (WT n = 116, Mut n = 11, $p< 0.62$), *IDH1* (WT n = 123, Mut n = 4, $p< 0.98$), *ASXL1* (WT n = 125, Mut n = 2, $p< 0.33$). Adverse karyotype was the only variable significantly associated with lower ITD clone count ($p < 0.001$), with mutated patients showing markedly fewer ITD clones compared to wildtype patients, suggesting that adverse cytogenetics and high ITD clonal complexity tend not to co-occur. (**F**) Scatterplot depicting the mathematical relationship between NGS-derived maximum allelic ratio (AR, log scale) and NGS-derived maximum VAF (log scale) across 125 *FLT3*-ITD-positive patients. The near-perfect correlation (Spearman $\rho = 1.0$) reflects mathematical equivalence between these metrics: $AR = VAF/(100-VAF)$. Both axes represent measurements derived from the same NGS sequencing run; this figure does not compare fragment analysis to NGS.